Journal of
Applied Remote Sensing

RemoteSensing.SPIEDigitalLibrary.org

Assessment of remote sensing-based classification methods for change detection of salt-affected areas (Biskra area, Algeria)

Gabriela M. Afrasinei
Maria T. Melis
Cristina Buttau
John M. Bradd
Claudio Arras
Giorgio Ghiglieri

SPIE.

Gabriela M. Afrasinei, Maria T. Melis, Cristina Buttau, John M. Bradd, Claudio Arras, Giorgio Ghiglieri, "Assessment of remote sensing-based classification methods for change detection of salt-affected areas (Biskra area, Algeria)," *J. Appl. Remote Sens.* **11**(1), 016025 (2017), doi: 10.1117/1.JRS.11.016025.

Assessment of remote sensing-based classification methods for change detection of salt-affected areas (Biskra area, Algeria)

Gabriela M. Afrasinei,[a,*] Maria T. Melis,[a] Cristina Buttau,[a] John M. Bradd,[b] Claudio Arras,[a,c] and Giorgio Ghiglieri[a,c]

[a]University of Cagliari, TeleGIS Laboratory, Department of Chemical and Geological Sciences, Cagliari, Italy

[b]University Wollongong, School of Earth and Environmental Sciences, Wollongong, New South Wales, Australia

[c]University of Sassari, TeleGIS Laboratory, Desertification Research Center–NRD, Sassari, Italy

Abstract. In the Wadi Biskra arid and semiarid areas, sustainable development is restricted by land degradation processes such as secondary salinization of soils. Being an important high-quality date production region of Algeria, this area needs continuous monitoring of desertification indicators, hence highly exposed to climate-related risks. Given the limited access to field data, appropriate methods were assessed for the identification and change detection of salt-affected areas, involving image interpretation and automated classifications employing Landsat imagery, ancillary and multisource ground truth data. First, a visual photointerpretation study of the land cover and land use classes was undergone according to acknowledged methodologies. Second, two automated classification approaches were developed: a customized decision tree classification (DTC) and an unsupervised one applied to the principal components of Knepper ratios composite. Five indices were employed in the DTC construction, among which also is a salinity index. The diachronic analysis was undergone for the 1984 to 2015 images (including seasonal approach), being supported by the interpreted land cover/land use map for error estimation. Considering also biophysical and socioeconomic data, comprehensive results are discussed. One of the most important aspects that emerged was that the accelerated expansion of agricultural land in the last three decades has led and continues to contribute to a secondary salinization of soils. [DOI: 10.1117/1.JRS.11.016025]

Keywords: land degradation; salinization; land cover mapping; decision tree; Landsat; change detection.

Paper 16666P received Sep. 10, 2016; accepted for publication Jan. 16, 2017; published online Feb. 10, 2017.

1 Introduction

Efficient soil and water management and sustainability of agricultural lands depend on regular monitoring of land degradation processes,[1] especially in arid and semiarid environments. The development of diversified production systems relies on the adaptation to drought and desertification, such as agroforestry techniques and ranching of animals better adapted to local conditions.[2] Therefore, to establish strategies for sustainable development and local and regional levels and to provide useful input for decision makers and stakeholders, constantly updated information on the ecological state of the territory is needed.

In this paper, we focus on the assessment of land degradation dynamics in the Biskra area of Algeria, characterized by an arid and semiarid climate. Because this area is highly vulnerable to increases in climatic variability and anthropogenic pressures, updated mapping and constant monitoring of land degradation indicators as well as identifying driving factors are critical,

*Address all correspondence to: Gabriela M. Afrasinei, E-mail: afrasinei.gabriela.m@ieee.org

1931-3195/2017/$25.00 © 2017 SPIE

as these withstand the understanding of desertification dynamics. Therefore, this work proposes an adaptive and replicable methodology and methods for the diachronic mapping of land degradation indicators, such as soil salinization. This analysis incorporates remote sensing techniques, two types of classification methods (visual and automated), and a large set of ancillary data. Its main objective is the assessment of a classification scheme that best copes with the issues risen by this type of study area and that can be reliable and easily replicable both in time and space (other environmentally similar areas). This analysis is finalized at the estimation of quantitative and qualitative change of land cover and the arguing of possible driving factors.

Land degradation and desertification represent the most severe environmental issues and key obstacles to meet ecological and human needs at global, regional, and local scales.[3–5] The recent Millennium Ecosystem Assessment Report indicates that desertification threatens over 41% of the Earth's land area; 20% to 70% of dry lands are already degraded, resulting in a decline in agricultural productivity, loss of biodiversity, and the breakdown of ecosystems.[6]

Chapter 12 of Agenda 21, as approved by the United Nations Conference on Environment and Development, defines desertification as a form of "land degradation in arid, semiarid and dry subhumid areas resulting from various factors, including climatic variations and human activities," triggering the losses of ecosystem services.[5,6] According to FAO (2016), land degradation is "the reduction in the capacity of the land to provide ecosystem goods and services and assure its functions over a period of time for the beneficiaries of these," especially due to land mismanagement.[3,7]

Common indicators of desertification include a decrease in land and soil properties and quality, and their ability to undertake their normal ecosystem functions, all of which lead to an increase in soil erosion and salinization.[2,7–9] They are also strongly linked to health and human development indicators,[6] which can also be employed to indirectly assess the dynamics of desertification (triggers, driving forces, impact, trends, and mitigation plans). The main drivers of desertification include deforestation, overgrazing, overcultivation, pressure of population, water usage, industrialization, and inappropriate land use practices.[5]

In the current study, we address the spatiotemporal dynamics related to land degradation and not soil degradation. It is important that a clear net distinction should be made between these two concepts. After a thorough literature review, Escadafal et al.[10] highlight that "land" must be approached through its multidimensionality, hence its sustainable management, including its biophysical components and their interconnectivity, but also the anthropic interfering. On the other hand, soils are a part of land, generally comprehended in biophysical terms through their vertical dimension. Therefore, when it comes to land, the issue of degradation and sustainability is dealt with at a landscape level (which can relate to sociology, anthropology, economics, etc.), while dealing with soil degradation will typically infer a focused and dedicated assessment having unique links with applied microbiology, biotechnology, optics, and even astronomy. Consequently, land is associated more with disciplines of the domain of social sciences, whereas "soil" has more connections with natural or physical science usually known as "hard sciences."[10]

Out of the various forms of land degradation, soil salinization is the main menace for sustainable agriculture worldwide.[11] It is estimated that more than half of the irrigated land in arid and semiarid regions of the world is affected to some degree by salinization and that millions of hectares of agricultural land have been abandoned because of salinity buildup.[11–14] Soil salinization is a process that leads to an excessive increase of water soluble salts in soil. The salts that accumulate include chlorides, sulfates, carbonates, and bicarbonates of sodium, potassium, magnesium, and calcium.[15] A distinction can be made between primary and secondary salinization processes. Primary salinization involves accumulation of salts through natural processes such as physical or chemical weathering of rocks and primary minerals, either formed *in situ* or transported by water (including groundwater) and/or wind. Secondary salinization is caused by human interventions, such as use of salt-rich irrigation water or other inappropriate irrigation practices, and/or poor drainage conditions.[15] In arid and semiarid areas, leached salts concentrate in slow-flowing groundwater and are brought to the soil surface through high evapotranspiration and their accumulation can also be accelerated as a result of anthropogenic activities, mainly through irrigation with saline water.[11] This is the case of the Biskra study area. The geological information is essential to the understanding and analysis of the salinity and salinization

mechanism, enhancing the prediction accuracy.[12] In the Biskra study area, the geological setting gives an *a priori* favorable background for the leaching and mobility of soluble salts, and their deposition in lower topographies.[16–18] Parent material, the type of soil, morphology, geographical location, and anthropic activities strongly influence the variability of soil salinity and trigger secondary salinization.[1]

Remote sensing was singled out as a useful tool for the detection and multitemporal analysis of desertification indicators for decision support, among numerous other applications.[19–21] Remote sensing infers the analysis of measured electromagnetic energy emitted or reflected by a target. A vast set of remote sensing data is available for salinity mapping and monitoring.[22] Classification of satellite images is one of the most commonly applied techniques used to process remotely sensed data, a method of creating meaningful digital thematic maps from imagery.

There are two commonly used remote sensing mapping methods. One involves visual photointerpretation based on professional knowledge, and the other one is represented by automated classifications based on the use of computers. Visual interpretation focuses more on the applications and the automated method more on technological research.[23]

In the Biskra area, field data were difficult to achieve in the correct amount needed for such studies, thus available ancillary data and other types of ground truth (GT) data were used as main support throughout the study phases.

In this study, we employ both visual and automated classification methods. The methodology used in this study derives from the need to tackle two core types of problems: (1) the conceptual environmental issue, hence soil salinity and secondary salinization and the challenge to correctly separate and describe each of them in terms of genesis and processes and (2) from the technical and methodological point of view, identifying or designing the appropriate classification approach, required spectral confusion among very reflective desert features, hence the limited or no access to field data or to undergo field survey oneself. We put forward this approach to cope with limited access to GT data and minimize misclassification issues reported in the literature regarding the correct delineation of land cover features in desert areas. Moreover, several researchers have emphasized the importance of a polyvalent or hybrid methodological approach for mapping and detecting changes spatially and temporally with an increased accuracy.[24–30]

In arid and semiarid areas, in particular, problems regarding automated image misclassification of high-albedo desert features have been reported by the scientific community. Among these, salt features classification issues also have been reported, either with supervised or unsupervised classifications, or with spectral mixture methods, mainly regarding spectral confusion of salt features with other land ones, especially urban fabric, bare soil, or carbonate-rich lithology.[11,12,19,31,32] To overcome the aforementioned issues, which are related not only to spectral confusion and misclassification but also to the difficult access to field data, two different classification schemes are approached in this study: (1) a DTC[12,33–37] and (2) IsoDATA classification applied to the principal components analysis (PC/PCA) of Knepper ratios.

In some situations, where the data are expected to have a normal distribution within each class, in a multispectral space, statistical image techniques are optimal for their classification.[37,38] However, these are known to be restrictive in resolving interclass mix-up if the data employed do not have a normal distribution.[35–37,39] Sophisticated statistical and neural/connectionist algorithms, rule-based classifiers, image segmentation, and support vector machines for both fuzzy and hard classifications of data have been developed during the 40-years lifetime of the remote sensing scientific community and are increasingly being used. Nonparametric classifiers have frequently been found to yield higher classification accuracies than parametric classifiers because of their ability to cope with nonnormal distributions and intraclass variation found in a variety of spectral data sets.[36,40,41,42] Decision tree classification (DTC) is one such technique, found to be very effective for the remote sensing community for land cover and land use (LULC) classification and salt-affected areas mapping, among a vast gamma of environmental applications.[12,32,33,35,39,40]

Consequently, in this study, we employ a customized decision tree classifier that copes with the aforementioned issues, managing to delineate correctly 12 land cover classes and differentiate between two types of salt-affected areas: highly and moderately saline. We employ new indices in the decision tree classifier,[43] which aim to cope with the issues risen by the study areas,

in terms of well-known spectral confusion of highly reflective land features in semidesert/desert areas. The choice of the DTC is thoroughly discussed in Sec. 4.3.

From a different point of view, soil salinity mapping through remote sensing is translated through the spectral characterization of the contained abundant salt minerals. Within the current study, we propose the employment of Knepper ratios composite for salt features identification, previously employed only for geological remote sensing analysis.[38,44] The reason why the latter one was also employed was to evaluate its potential as an approach of fast automated, user-independent spectral-based classifier, as opposed to decision tree analysis that needs thorough computation for rules choice and threshold calculation.

In this study, we have employed historical and present Landsat imagery for the diachronic analysis of salt-affected areas. The scientific literature has shown that either multispectral or hyperspectral imagery have yielded optimal results for the detection and mapping of salt features.[20,21,45–48] However, the various shortcomings of both imagery sets preserve "no agreed-on best approach to this technology for monitoring and mapping soil salinity."[21] Despite researchers being hesitant in using multispectral imagery for salinity mapping because of several drawbacks, this type of image has been stated in the literature to be preferred for mapping and monitoring soil salinity.[49] Furthermore, several authors[20,32,49] have indicated multispectral imagery to be relevant for such studies, as well as much more accessible and affordable [freely downloadable from US Geological Survey (USGS) platforms], e.g., considering the broad nature of Landsat sensors and its time spread, not to mention that it is the most common type of imagery cited in numerous publications and not limited to saline features analyses.[12,50,51,52]

In previous studies, likely problems of mixed pixels or limitations have been accounted for through ancillary data inputs such as field data, *in situ* measurements and sampling for adjacent analysis, or through the integration with geographic information systems (GIS), and digital elevation models.[53,54] In this work, we have used a large set of ancillary data either for training data or for the validation of outcomes. This set of data is described in detail in Sec. 2.2.

In the following section, the study site and the materials and dataset employed are described. Section 3 presents the methodology and description of the mapping methods applied in this analysis.

The final objective of this paper is the engagement of remote sensing imagery in change detection in an area presenting specific restraints, both environmentally or from the accessibility point of view; hence, a consistent number of works have been reviewed for the current study that discuss or use satellite imagery[26,52,55,56] which reported issues regarding discrepancy of results and the degree of the replicability of algorithms or methods applied.[57] We tried to minimize these issues through the proposed aforementioned methodology and approaches described in the following sections. In this study, we also consider seasonal variation (wet versus dry season) to assess to what extent and degree this theory applies in this case study because the importance of seasonality on salt features delineation is reported in the literature in several works.[12,20,58,59]

This study is part of the Water harvesting and Agricultural techniques in Dry lands: an Integrated and Sustainable model in MAghreb Regions (WADIS-MAR) Demonstration Project, funded by the European Commission through the Sustainable Water Integrated Management Program.[60] The project aims at the promotion of an integrated, sustainable water harvesting and agriculture management, and at the extensive dissemination of sustainable water management policies and practices in two watersheds in Tunisia and Algeria.[61]

2 Dataset

2.1 *Study Site*

The study site is located between the Saharan Atlas and the Saharan Plateau in Algeria, north-northwest of the great Chotts of Melrhir and Felrhir, and covers an area of about 5000 km^2 (Fig. 1). It represents mainly a piedmont area that passes from the Aures mountainous and hilly domain in the north to the Sahara plain in the south, with fine clayey deposits and vast alluvial fans and small mountain ranges in the middle slope area.

The area can be divided into two zones: the "Occidental Zab" and the "Oriental" one (as shown in Fig. 1), where Wadi Biskra constitutes the limit between the two zones. Locally

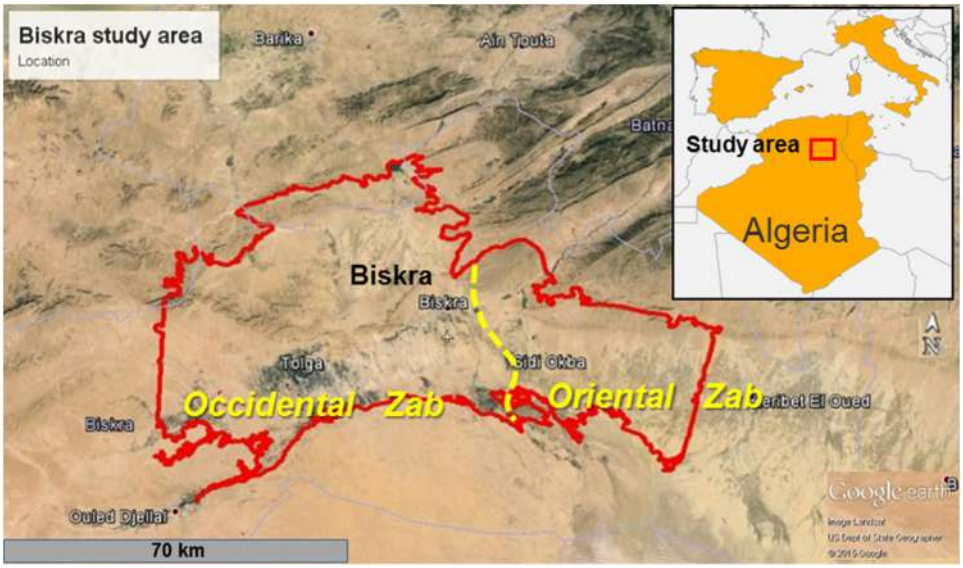

Fig. 1 Biskra study area (modified from Google Earth, 2015). The WADIS-MAR project partners are highlighted in orange in the upper-right image of location overview.

known as the "Zibans palmeraie" (palm grove) or the Occidental Zab, the irrigated area exceeds 65,000 ha and draws more than 600 million of m^3 per year, whereas the Tolga area is an international exporter of high-quality dates "Deglet Nour." The high productivity of these palm groves is due mostly to the presence of very productive and shallow aquifers highly exploited for more than one century, with an average salinity from 2 to 4 g/l; hence, the increase of surface salinity and gypsum encrusting. The land use mainly regards date palm plantations and extended greenhouse cultivations (vegetable cultivations), followed by open field cultivations.

The landscape of the Oriental Zab domain is characterized by vast alluvial fans and a plain modeled by wadi courses, with their source area in the Atlas and eventually fading into the great depression of the greater watershed of Chott Melrhir, reaching an average of −80 m below sea level.[62] Open field and industrial cultures have become an intense practice in the last decades, as these ones, unlike "phoeniciculture" (French word for "date palm cultivation"), do not require a shallow aquifer,[63] but the usage of deep groundwater has increased in the last decades.

From the geological point of view, the Biskra area is located in the transition zone between the folded Atlas domain in the northern part of the area and the desert and flat domain of Sahara in the south. The area is characterized by the superposition of several folding events occurring from middle Eocene to Pleistocene, which strongly influence the geometry of the main aquifers.[64–66] The lithological stratigraphy is composed mainly out of clay and sand alternations (Quaternary and Mio-Pliocene), gypsum clays and evaporitic deposits (middle Eocene); limestone (lower Eocene); limestone, gypsum clays, and halite (Senonian); dolomitic limestone and dolomites (Turonian) and clay, marlstone, and gypsum belonging to Cenomanian; and Triassic salt domes.

Gypsiferous and calcareous soils are two important groups of soils formed in arid and semiarid environments of Algeria.[18] In most cases, gypsum is associated with other salts of calcium, sodium, and magnesium. All these minerals have an average solubility in water, and because of this solubility, these minerals are altered easily and can be deposited in other places and in other mineral forms. Most soils in this study area are composed of gypseous soil, or gypsum ($CaSO_4 2H_2O$), which is common in geological materials, groundwater, and surface area.[18]

The climate is hot and dry, stretching over the semiarid, arid, and predesert zones, with an annual maximum average of about 28°C. The maximum frequency of rainfall is in November and March, and the total annual rainfall average is about 150 mm, but the annual mean rainfall is <20 mm. The minimum rainfall is almost null in the months of July and August.

2.2 *Materials and Data*

A large set of ancillary data was used for the visual photointerpretation phase of the LCLU classes, comprising available spatial data, geological and topographical maps, agricultural calendars, statistics, and pedological reports, mainly provided by local entities and institutions, such as "L'Agence Nationale des Ressources Hydrauliques," Algeria (ANRH), "Institut Technique de Développement de l'Agronomie Saharienne," and other local entities. Available Google Earth high-resolution satellite images and data were also consulted and partially used for the generation of GT data. The community-based Google Earth photographs and information were also employed as ancillary data in order to have a general acquaintance with the study area, an input on ground data, land use, and overall landscape (high-quality imagery of Google Earth Pro). Nevertheless, error potential and debatable reliability were taken into account, given that this crowd-sourcing data include nonexpert users.

The Landsat data were obtained by the courtesy of the USGS web platforms. All the images of the years available for this area were consulted, and only the ones presenting good quality and low cloud coverage were chosen for this study. The images from 1984 to 2015 were chosen as presented in Table 1. They were also chosen avoiding exceptional or abnormal humid years (abnormally higher than the average total annual precipitations of the past 40 years), which were irrelevant for this study as it could bias the study results. The imagery at the beginning of the dry season and at the end of it was chosen based on climate data, avoiding abnormal rainy years, days, or rainy periods prior to the selected dates. For example, when selecting the images acquired at the end of the dry season, it was important that prior to that date no abnormal rainy days or periods took place: if the acquisition date was the third of September, but on the second or first, there were 20 mm of precipitations, we considered that the data would have been compromised if analyzed. The choice of the scenes was mostly restricted by cloud coverage. ArcGIS 10.2 was employed for geospatial data consultation and geoprocessing and ENVI 5.2 Software (Exelis VIS, Boulder, Colorado) was used for the satellite data preprocessing and processing and postclassification.

As this study approaches an inter- and intraannual change analysis, two images per each one of the 4 years were chosen: one at the beginning and one at the end of the dry season. This can be argued by the fact that there is a maximum vegetation peak at the end of May, after the winter–spring rainfalls and a minimum vegetation peak at the end of the dry season, in August to September, which can restrain or aid the identification of saline areas, respectively.[12,21] We have taken into account the fact that, in these particular areas, the visibility and reflectance intensity of various types of land cover types and especially salt features are influenced by seasonality, potentially compromising their correct identification and delineation. According to studies conducted in similar biophysical and climatic conditions and presenting analogous research

Table 1 Landsat scenes employed in the diachronic analysis.

Satellite	WRS path	WRS row	Acquisition year	Day of acquisition—Julian day number (JDN)	Date
LT5	194	36	1984	182	June 30
LT5	194	36	1984	246	September 2
LT5	194	36	1995	148	May 28
LT5	194	36	1995	228	August 16
LT5	194	36	2007	149	May 29
LT5	194	36	2007	229	August 17
LT5	194	36	2011	160	June 9
LC8	194	36	2015	123	May 3
LC8	194	36	2015	219	August 7

purposes, the most appropriate period for satellite data choice is the end of the dry season.[11,12,14,20,32] Therefore, in this study, we also consider this seasonal variation in order to assess to what extent and degree this theory applies in this case study, nonetheless being an arid, predesert environment.

The years were chosen at an interval of about 10 years, according to possibility, starting with 1984, the oldest one available (depending on sensor type, image quality, cloud coverage and validity for analysis). These were chosen after a careful consultation of climate data (Biskra weather station[67]) to avoid preceding heavy rainfall days, especially for the postdry season dates. The 2011 scene used for visual interpretation was not inserted in the multitemporal analysis, being used only for comparison purposes, through error assessment.

3 Mapping Methods

3.1 *Visual Interpretation*

Tackling environmental issues requires a thorough knowledge of the landscape and territory. Land use is associated with human activities that are directly linked to the functionality of the land, while land cover designates the natural elements as well as artificial structures covering the land surface. Constant update of land cover information, not to mention the land use one, is indispensable due to constantly changing geospatial phenomena over time, required particularly by various authorities engaged with the management of territory. However, it is important to highlight that planners and land managers need high accuracy of data to approach land cover problems appropriately, thus a constant improvement of the methods of collection, treatment, and interpretation of data is also due. Although the priority is land use mapping, as an analogue of economic information, it cannot be easily mapped, as opposed to land cover, which is more handy and can serve as an estimation of land use.[68] Automated classifiers usually manage to extract land cover information based on spectral response. Other input data and expert knowledge are usually needed to associate the land cover features to land uses. In an image classification, the spectral components alone cannot provide information on land use, unless they have obvious characteristics (e.g., rectangular-like pattern of cultivated parcels) that would indicate land use.

For the current study, the LCLU map assisted as reference data for the overall acquaintance with the study area. The visual photointerpretation method is an acknowledged one due to its detail, quality, and expert knowledge validity,[23,69] and in this study, it was constructed according to standard and acknowledged methodology,[70–73] employing a large set of ancillary data, using 1 : 40,000 mapping scale and 25 ha minimum mapping unit (MMU). A total of 37 LCLU classes of fourth level of detail (according to CORINE land cover)[73] was obtained. The methodological and classification approaches were adapted from various land cover programs implemented either in Europe, such as CORINE land cover, or in the African ones.[70–72] These allowed us to define visual interpretation keys and variables and build a land cover nomenclature and class description tailored to the local context. In the Biskra area, the interpretation of the Landsat TM5 of June 9, 2011, path 194, row 36 resulted in 37 LCLU classes that were defined based on a large set of ancillary data, of both analogical and digital data, given that GT data were difficult to obtain with the necessary detail and amount (around 50 GT points were acquired). The generation of this map allowed us to properly plan the field survey in both areas. Thus, doubt points were selected, and material was prepared (GT sheets, point location basemaps containing the doubt points to be verified in the field) and sent to the local WADIS-MAR partners, which delegated experts in the area of study to undertake the field verification of points. The field survey allowed us to verify and correct previously interpreted polygon boundaries and verify class nomenclature and the assignment of class names to polygons. A flowchart is provided in Fig. 2, illustrating the main phases of the adopted methodology.

3.2 *Data Preprocessing*

The level L1T products were a subset to the study area extent, radiometrically calibrated to obtain top of atmosphere reflectance, and, subsequently, dark object subtraction was applied

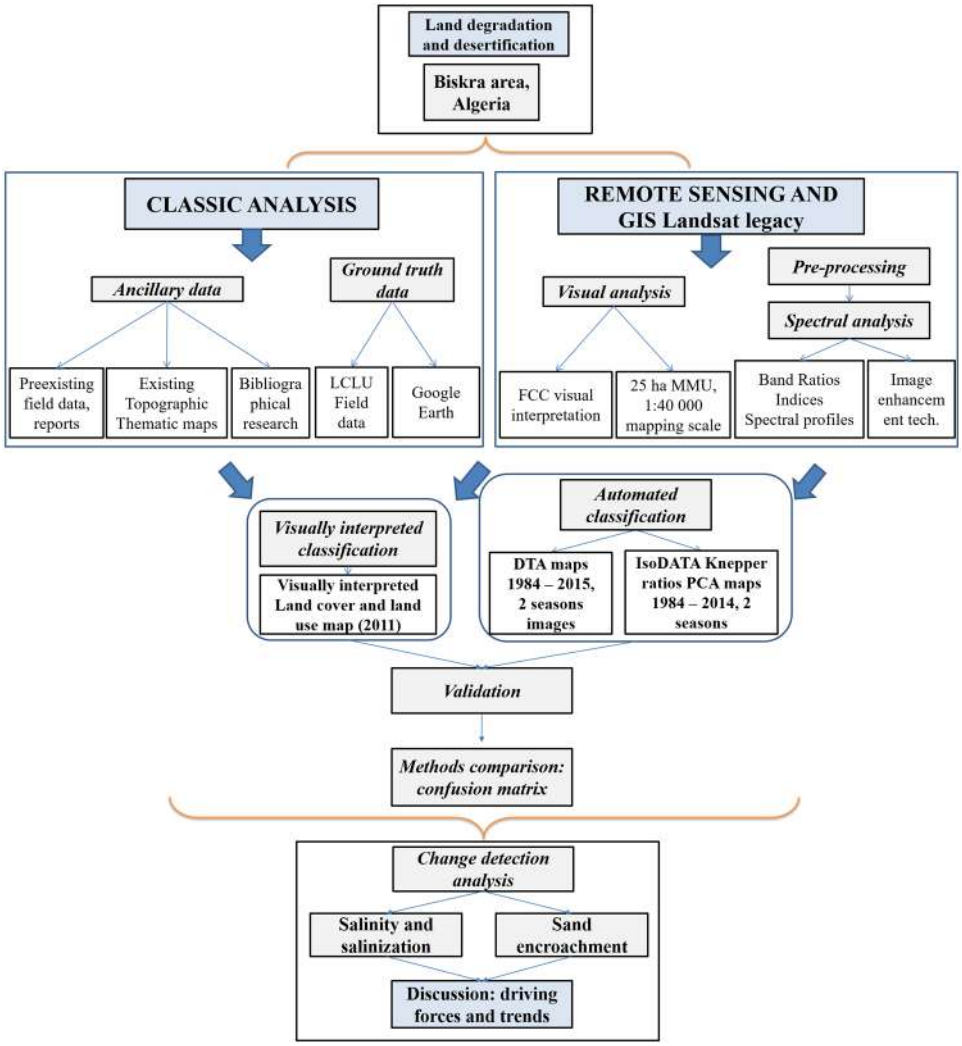

Fig. 2 Customized methodological workflow.

for atmospheric correction, thus obtaining surface reflectance. As the product employed ground control and relief models (as delivered by the provider, namely USGS), geometric correction was not performed.[68,74] No topographical correction was applied as it has been reported by several authors as prone to overcorrect values in plain areas and lose valuable information, especially in regions where spectral separability has such sensitive thresholds.[75,76] All images were verified for coregistration.

3.3 *Decision Tree Analysis*

In remote sensing, choosing a classification approach, method, or algorithm (image classifier) must be made upon specific criteria that take into account the aim, type, and object of the study, feature to classify (associate each pixel to a class) and identify (relate classes to a known land cover/use), data dimension, computation requirements, time, costs, etc. Since the present study is targeted at a change detection analysis, thus a multitemporal study of land features (not clouds or aerosols), at a local–regional scale (5000 km^2, around a third of the Biskra Wilaya), and given the employment of medium resolution multispectral imagery, a decision tree type classifier was evaluated as being the optimal one. In the following paragraphs, this choice is argued both in technical (digital image processing techniques) and in conceptual (spatio-contextual information) terms.

Conventionally, classification tasks are based on statistical methods and some of the most common classification algorithms include (supervised/unsupervised) minimum

distance-to-mean, maximum likelihood, Mahalanobis distance classification, nearest neighbors, or IsoDATA.[77,78] Traditional classification procedures like maximum likelihood classifiers are generally based on statistical parameters, such as mean and standard deviation. Generally, these classifiers are based on an explicit underlying probability model that provides a likelihood of data belonging to a particular class rather than simply a classification, and its performance is determined by how well the data match the predefined model. Furthermore, it has been proven that modeling the data appropriately can become a real problem if these data are complex in structure.[35,79]

To overcome these issues, more advanced classifiers like artificial neural networks, fuzzy classifier, image segmentation, expert classification, support vector machines, rule-based classifiers, and many others are increasingly being used.[35] These techniques are mainly characterized by the lack of any preliminary supposition on the data distribution, especially because they are nonparametric.[39] The ability to cope with nonnormal/nonhomogeneous distributions and intraclass variation found in a variety of spectral data sets rendered nonparametric classifiers superior in yielding higher classification accuracy when compared with the parametric ones.[41,42,80]

DTC techniques, either manual or automatic, have been used successfully for a wide range of classification problems, but only recently tested in detail by the remote sensing community.[33,36,37,39,40,81] Several studies have compared DTC methods with other classifiers. Otukei and Blaschke[40] compared an automated decision tree (using data mining approaches for calculating thresholds), maximum likelihood, and support vector machine-based techniques for land cover change assessment using Landsat TM and ETM+ data and found decision tree-based methods performed better than others. Other studies compared decision trees, support vector machines, and random forest methods, resulting in equal performance, whereas others employed automated decision trees, such as C5.0-based DTC (data mining tool, an improved algorithm following C4.5) to classify IRS-P6 AWiFS (Indian Remote Sensing ResourceSat-1 Advanced Wide Field Sensor) data, and reported very high accuracy.[39]

Even if decision tree algorithms have been shown to perform less well in higher dimensional feature spaces when compared with maximum likelihood classifiers, several studies demonstrated that they still outperform it.[40,42] For instance, Srimani and Prasad[35] concluded that DTCs are capable of automatic feature selection and complexity reduction, providing interpretable information regarding the predictive or generalization ability of the data. Furthermore, they also showed that DTC is computationally time-efficient and that some of the popular machine learning DTCs tested in their study have presented high potential in providing accurate and efficient classification of LCLU mapping employing remote sensing data.

In the present study, the decision tree analysis was chosen because of its high flexibility of input data range and easiness of class extraction through multistage classification but at the same time because of its simplicity, hence its hierarchical structure of nodes, their explicit connections and status for class separation, their significant intuitive appeal and easy interpretation.[37,68] This choice can be argued, as presented in existing literatures, through the fact that decision trees offer high ability to handle data measured on different scales, lack of any assumptions concerning the frequency distributions of the data in each of the classes, flexibility, and ability to handle nonlinear relationships between features and classes. The possibility of incorporating various types of data sources under a single-classifier framework proved to be advantageous in using DTC. In contrast to neural networks, decision trees can be trained quickly and are rapid in execution. They can be used for feature selection/reduction as well as for classification purposes. Because it is easily interpreted, it is not a "black box," like the neural network, the hidden workings of which are concealed from view.[33,36]

When the analyzed data are too complex in nature, data mining DTCs, or other algorithms employed for training of automated DTCs, are inappropriate for determining decision thresholds, thus manual decision trees are "safer." Traditionally, the thresholds are obtained using the knowledge provided by experts who employ their expert knowledge to assess and create the decision boundaries. When expert knowledge required to determine the decision boundaries is lacking, it provides challenges for image classification and it is in this case that data mining algorithms prevail.[40]

3.4 *Decision Tree Classifier Construction*

This manual DTC construction phase consisted of thorough spectral analysis using spectral enhancement techniques, horizontal and vertical spectral profiles analysis, and 2-D scatter plots investigation of salt features to understand their spectral behavior in relation to features that can present similar spectral characteristics and confusion: carbonate-rich and clay-rich areas, bare land, urban fabric and outcropping rocks, and a large set of ancillary data.[32,82,83–85] After reviewing several vegetation and salinity indices reported as successful in delineating salt-affected areas,[20,21,86] the results that emerged were not completely satisfactory and further analysis was undertaken to choose optimal band operations for decision tree integration. For the spectral analysis phase, we have taken into consideration two factors: one is the maximum information content of the composite bands (the higher the standard deviation is, the more information content is derived from the composite bands) and the other is the minimum affinity of the composite bands leading to significant independence and less redundant data (high covariance between bands).[87,88] Consequently, band ratios and indices[20,89,90] have been derived to discriminate as accurate as possible the features of interest and to support decision rules used for a DTC scheme. The indices proposed for this study are constructed based on choosing optimal band pairs/groups, which have high spectral information covariance of each land feature of interest. Identifying optimal bands for building indices is also accounted for through methods like optimum index factor (OIF) or correlation analysis between *in situ* measured spectral reflectance and satellite data.[87,91] For example, in the case of "highly saline areas" class extraction, Landsat visible bands of blue, green, and red information are usually put together, as they present high correlation, in order to enhance the "brightness" features. They are subsequently divided by band SWIR2, which presented the lowest reflectance values of salt features, hence high covariance with the three aforementioned. This can be argued by the fact that the spectral behavior of salt minerals ($CaSO_4 2H_2O$, $CaCo_3$, NaCl, etc.) is related to molecule vibration fundamentals, overtones, and combinations, which can generate vibrational or absorption bands in the infrared region due to OH, CO_3, and H_2O.[92] A vibrational absorption will be seen in the infrared spectrum only if the molecule responsible shows a dipole moment (it is said to be infrared active). Water and OH (hydroxyl) produce particularly diagnostic absorptions in minerals. In fact, the spectral confusion of saline gypsum-rich areas with carbonate-rich areas is rightful since the combination and overtone bands of the CO_3 fundamentals occur in the near-IR.[92]

The resulting indices related to highly and moderately saline areas extraction are thus expressed as: $\text{sqrt}\{[(b12)+(b22)+(b32)]/b7\}$ or $(b1+b2+b3)/b7$, salt minerals index and salinity hue index.

Exponential or square root functions were used to force the emphasis of extreme values, helping in delineating high or moderate saline areas. The statistics of each index/math image were used to establish the thresholds for each decision node.

3.5 *Knepper Ratios and Principal Component Analysis*

Knepper (1989)[93] proposed specific band ratios for the delineation of hydroxyl-bearing minerals, hydrated sulfates and carbonates, vegetation, and iron-oxides and hydroxides using Landsat TM bands, namely the red–green–blue (R:G:B) composite of ratios 5/7:3/1:3/4 (where 5/7, 3/1, and 3/4 are ratios of the TM bands 5 and 7, 3 and 1, and 3 and 4, respectively), used mainly for geological remote sensing mapping. Other ratio RGB combinations, such as Gozzard ratios 5/7:4/7:4/2 are known to be prospective for iron, chromium, nickel, and platinum group metal resources.[44] The Abrams ratios (5/7:3/2:4/5), Kaufmann ratios (7/4:4/3:5/7), and Chica–Olma ratios (5/7:5/4:3/1) are successful in the identification of minerals containing iron ions, hydrothermally altered iron-oxide, clay minerals (and altered), hydroxyl minerals or vegetated zones, and ferrous oxide.[89]

The PCA was applied to Knepper composites of each year[44] to obtain a fast spectral separation of main land cover types and especially to rapidly identify areas with different lithology and mineralogy. It was employed to evaluate its potential as an approach of fast automated, user-independent classifier, as opposed to decision tree analysis that needs thorough computation for rules choice and threshold calculation. It is based only on the spectral information contained

within the employed bands, but it does not allow other manipulation, which was considered by us rigid, as it presents a consistent problem of mixed pixels. In fact, the obtained images presented difficulty in applying a classifier and to avoid further errors, IsoDATA unsupervised classification was chosen, as it proved to be the most suitable, with a maximum of 50 iterations, a threshold of 2% and 12 classes requested. The PCA analysis was applied for each one of the nine assessed years.

4 Results and Discussion

4.1 *Visual Interpretation Land Cover and Land Use Map*

A total of 37 LCLU classes of fourth level of detail (according to CORINE land cover[73]) was obtained. The resulting map is shown in Fig. 3. The correspondent LCLU class nomenclature to the legend codes in Fig. 3 is provided in the Appendix (only the fourth level classes are given here, the upper levels correspond to standard CORINE nomenclature levels,[73] class description is not provided here).

4.2 *Decision Tree Classification*

The spectral indices and band math operations that resulted from the DTC analysis are shown in Fig. 4 and Table 2, respectively. Finally, the decision tree map was obtained by applying vegetation, wetness, mineral and salinity indices, and simple band ratios (Table 2), mostly derived not only from the analysis of bands statistics, scatter plots, and vertical and horizontal profiles of interest features but also from literatures. It is important to mention that the hierarchical order of the nodes (indices) is essential in the correct extraction of the land cover classes. For example, the fact that "highly saline areas" are extracted through the fifth node (before alluvial, carbonate-rich areas, and urban fabric) eliminates the possibility of other classes to overlay it, and thus

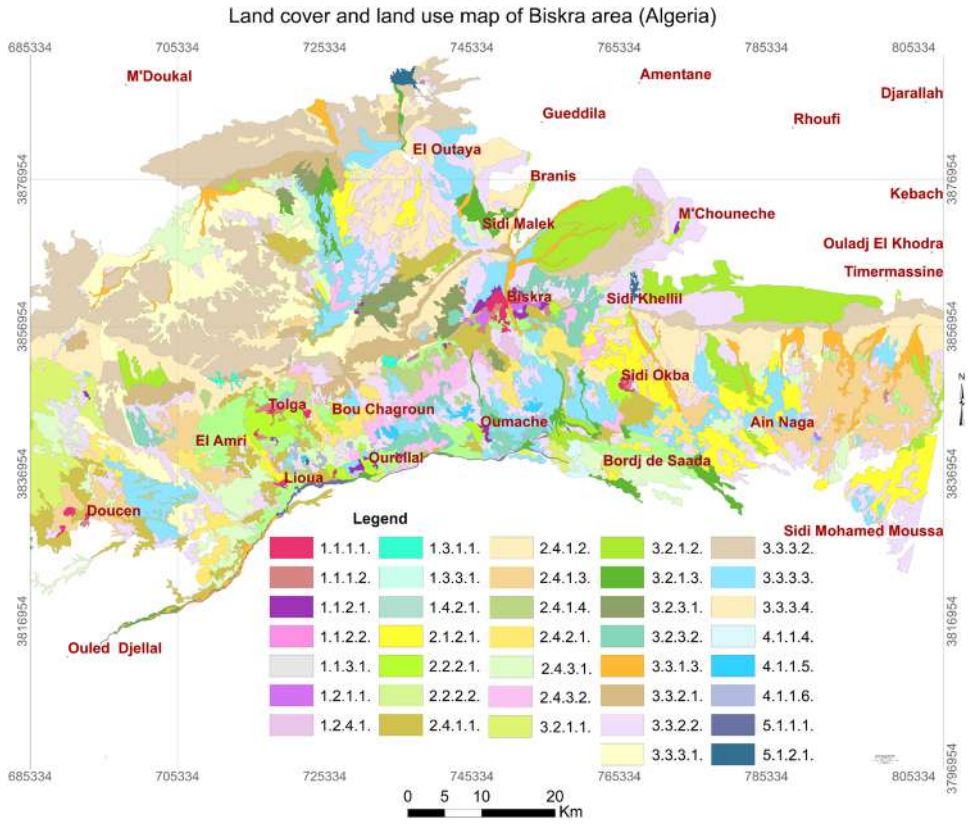

Fig. 3 LCLU map of Biskra area (built through visual interpretation).

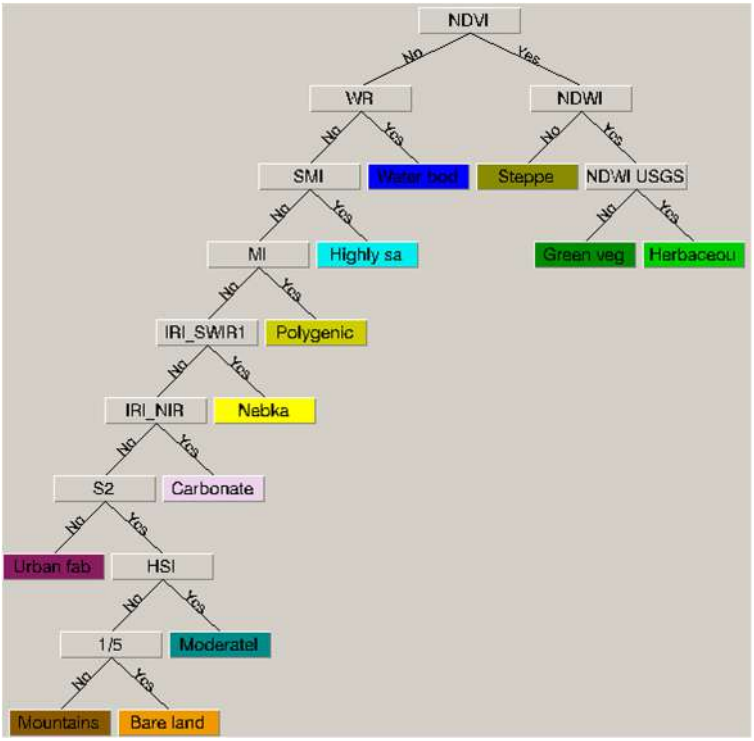

Fig. 4 Decision tree binary decision nodes and resulting classes.

Table 2 Indices analyzed for the decision tree construction in the study area. Thresholds correspond to the indices applied to the Landsat image of September 2, 1984.

Parent nodes decision	Expression	Band math (TM bands)	Indices	References
NDVI	$b1$ GE 0.175	$(b4 - b3)/(b4 + b3)$	Normalized difference vegetation index	14
NDWI	$b2$ GE −0.049	$(b4 - b5)/(b4 + b5)$	Normalized difference water index	63
NDWI USGS	$b3$ GE −0.267	$(b3 - b4)/(b3 + b4)$	Normalized difference water index—USGS	64, also known as normalized difference salinity index (NDSI) (31)
WR	$b4$ GE 1.01	$b3/b4$	Water index	Derived from Ref. 65
SMI	$b5$ GE 0.710	$\text{sqrt}\{[(b1\hat{2}) + (b2\hat{2}) + (b3\hat{2})]/b7\}$	Salt minerals index	Proposed for this study
MI	$b6$ GE 0.0263	$(b1 * b2 * b3)/b4$	Mineral index	Proposed for this study
IRI_SWIR1	$b7$ GE 0.85	$\text{sqrt}\{[(b4\hat{2}) + (b7\hat{2})]/b5\}$	Infrared index–short wave infrared 1 (TM band 5)	Proposed for this study
IRI_NIR	$b8$ GE 1.8	$sqrt\{[(b5\hat{2}) + (b7\hat{2})]/(b4\hat{2})\}$	Infrared index–near infrared (TM band 4)	Proposed for this study
S2	$b9$ LE −0.328	$(b1 - b3)/(b1 + b3)$	Salinity index 2	14
HIS	$b10$ GE 1.89	$(b1 + b2 + b3)/b7$	Salinity hue index	Proposed for this study
1/5	$b11$ GE 0.25	$b1/b5$	Ratio 1/5	60

Table 3 Description of the resulting class of the DTC.

Green vegetation	Oasis vegetation, mainly palm groves, fruit trees plantation, types of small trees and tall shrubs rich in biomass or chlorophyll
Herbaceous vegetation	Annual crops, small natural herbaceous vegetation, small shrubs
Steppe	Typical dry shrub vegetation, woody correspondent to mountainous and piedmont areas
Water bodies	Water areas of natural or artificial origin
Highly saline areas	Areas rich in salt minerals components
Bare soil (alluvial deposits)	Deposits correspondent to alluvial fans, recent alluvial deposits, piedmont and glacis accumulations, with a strong clay, sand, and coarse materials component
Nebka	Typical semiarid phytogenic aeolian coppice dunes, areas of sand plains (dunes) covered by sparse or very low vegetation
Bare soil (carbonate rich)	Areas with a high carbonate component, limestone crust, outcropping limestone
Urban fabric	Artificial, build-up surfaces, usually impervious
Moderately saline areas	Areas that present moderate salinity
Bare rock (calcareous)/mountains	Mountain ranges and slopes, scree, cliffs, including active erosion flats, outcropping bedrock
Bare soil	Land with no vegetation cover and of no land use

generate misclassification. Through the DTC, we managed to extract a higher number of land cover classes (12) than the average low number of classes (commonly between four and seven classes) usually obtained through traditional classification schemes at local–regional scales.[23,24–26,94,95]

The decision nodes and the resulting map are thus obtained for each of the eight dates. According to the lithological and vegetation cover of the area, the DTC and legend were adapted to classify the main land cover classes and classes of lithology distinguishable according to their spectral lithological response, which are described in Table 3.

4.3 *IsoDATA of Knepper Ratios Principal Components Analysis*

The results showed that the third principal component mostly contained salt minerals-related information. The first component, representing the highest covariance between the three ratio images, mostly contained important information on the sand component, and the second one, clay minerals, which mostly overlaid areas of alluvial fans, with loam and clayey components. The IsoData classification has presented difficulty in delineating the requested 12 main classes, some of which present similar characteristics to other existing ones, being unable to separate the "moderately saline areas" class. In order to allow comparison between the two sets of classification, the resulting DTC images to IsoDATA Knepper PCA classification images, the classes were evaluated for correspondence and the "improper" classes were not considered for analysis. In Figs. 5 and 6, the classes that do not correspond to the expected resulting classes are presented in white–gray–black levels, and the class name denotes the fact that it is more likely to belong to that one. Thus, for their comparison, only "highly saline areas" class was considered and the other ones were merged into one class of "land" for both DTC and IsoData maps.

4.4 *Validation and Methods Comparison*

The 2011 LCLU map was considered as "GT map" due its "three-in-one" validation merging multisource GT data: (1) field acquired data (50 points of various land cover types), (2) 100

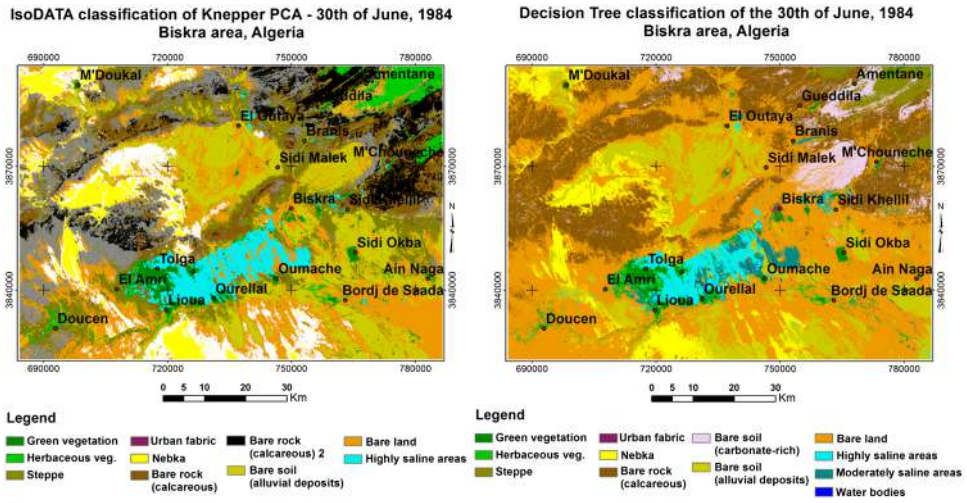

Fig. 5 IsoDATA classification applied to Knepper ratios PCA and DTC classification of June 30, 1984, image.

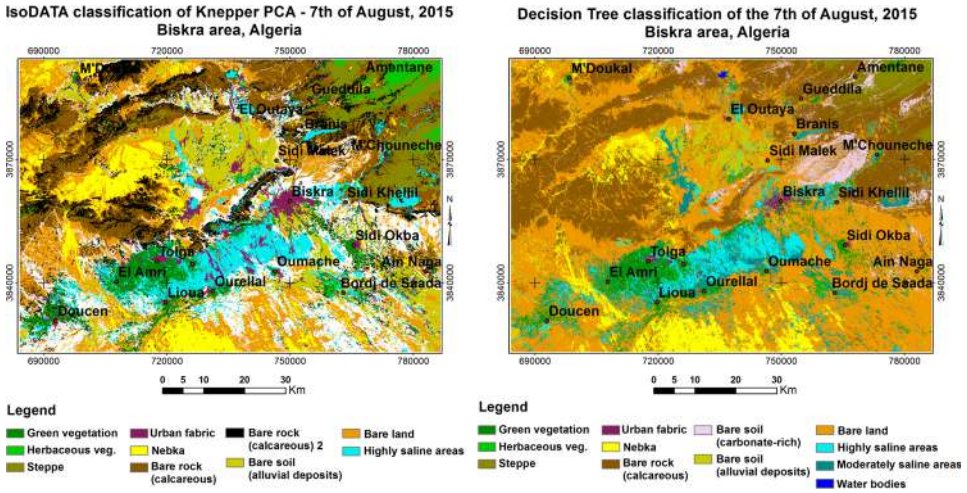

Fig. 6 IsoDATA classification applied to Knepper ratios PCA and DTC classification of August 7, 2015, image.

points extracted from a detailed pedological report (provided by ANRH, Algeria, indication various land cover types), and (3) 50 community-based GT points of various land cover types extracted from Google Earth. A fourth contribution to its validity is the expert knowledge input and the amount of interpretation keys (over seven variables) used for its construction. The GT points were used to generate GT regions of interest and to validate the LCLU map, presenting an overall accuracy of around 96% and a kappa coefficient of 0.88. The detail and the different types of GT data were appropriate for the validation of the 37 LCLU classes, since these classes, in their turn, were quite specific and detailed. However, the GT data were too heterogeneous to be used "as is" for the DTC map validation; we have merged all the GT data and expert knowledge into the LCLU map, and we used it as GT image in the confusion matrix process.

All classes were considered for qualitative and comparison visual inspection with other classifiers' results. However, for the quantitative comparison with the 2011 DTC and Knepper PCA results, only the saline areas classes ("highly saline" and "moderately saline" classes) were merged and taken into consideration. For the 2011 images, the accuracy assessment of the automated methods relative to the LCLU visually interpreted map is presented in Table 4.

Confusion matrix was also applied for the comparison among classification methods. This analysis was applied for the June 30, 1984, the June 9, 2011, and August 7, 2015, maps. The 1984 pair of DTC and IsoData Knepper PCA maps (Fig. 5) showed a rather good overall

Table 4 Comparison of DTC with IsoDATA of Knepper PCA map (date expressed in year_JDN).

	1984_182	2011_160	2011_160	2011_160	2015_219	2015_219
Classification methods pairing	DTC and IsoData KnepperPCA	DTC and LCLU visual interpretation	IsoData KnepperPCA and LCLU visual interpretation	DTC and IsoData KnepperPCA	DTC and IsoData KnepperPCA	DTC and Google Earth points of 2015 images
Employed classes	Highly saline areas	Highly saline areas	Highly saline areas	Highly saline areas	Highly saline areas	Various land cover types
Kappa coefficient	0.81	0.71	0.22	0.45	0.62	0.83
Overall accuracy	98.38%	97.06%	95.95%	95.03%	93.93%	86.88%
Producer accuracy	79.75%	78.64%	42.92%	48.57%	57.70%	67.70%
User accuracy	85.90%	30.28%	16.96%	45.78%	77.23%	80.21%

similarity of 98.38% and a kappa coefficient of 0.81, with good producers and user accuracies (in this case of comparison, inferring the consistency between the two maps); the 2015 pair (Fig. 6), on the other hand, has given an overall accuracy of 93.93% but a kappa coefficient of 0.62, as presented in Table 4. This discrepancy may be related to the disadvantages of the IsoData classification method, its threshold set for class separation and number of iterations, and the different quality of satellite data (Landsat 8), either in terms of noise or radiometric resolution. In fact, it must be mentioned that the 2015 images were more responsive to the application of the DTC possibly due to the higher radiometric resolution, instrument calibration, and product generation (level 1 products). For example, the only land cover class that has given difficulties in classification in all images was the "urban fabric" class. However, when DTC was applied to the 2015 images, these problems decreased substantially up to nonexistent. In fact, the 1984 images were laborious in node thresholds calculation, being very different from the rest of the images, whereas the other seven images have maintained very close threshold values of correspondent indices. For the 2015 DTC map, an accuracy assessment using GT data of various land cover types extracted from Google Earth images of 2015 (mosaic varying from August to December) was undergone. Since the DTC map was generated from the image of August 2015, we selected only the points (a total of 30 points) related to images acquired around the month of August.

An important aspect to be emphasized is the fact that the decision tree offered more flexibility, as a multistage classifier, thus managing to delineate classes with higher control. The amount, complexity, and types of spectral information put together in this single classifier make it highly controllable, as opposed to other classification flows. The comparison with the visually interpreted land cover map was undergone through visual inspection for all classes, but for a quantitative assessment, the DTC map of 2011 was reduced to only two classes: "land" and "highly saline areas" and compared with the "saline areas" class of the LCLU map. Error matrix showed a matching of 72%, which can be due to the subjectivity of the user, since visual interpretation implies a series of variables taken into consideration by the user when delineating features (contours, hue, size, texture, and location), but cannot allow the delineation of moderately saline areas. This class has a particular spectral response, not discriminative enough through visual interpretation, but only through spectral information extraction, i.e., an adequate index.

4.5 *Change Detection Analysis*

As a result of the DTC, we obtained the salinity/land cover maps for the chosen dates, as presented in Figs. 7–10, with a successful distinction of a total of 12 classes. We applied the

postclassification approach, which is the comparative analysis of independently produced classifications for different dates.[96–99] This method usually allows more complex legends to be used and, consequently, more detailed analysis of LCLU.[100] This methodology requires each of the classifications to have high accuracy, a goal not always reached when a legend with several agricultural categories is needed. In addition, it becomes more difficult in fragmented landscapes like the study area.[100] The drawback of this method is that it reduces the useful area of comparison, in the example case, substantially. However, the different classification accuracies, fragmentation of the landscape, planimetric accuracies, and pixel size are taken into account; therefore, in a future study, it would be interesting to assess the performance of other change detection methods.[101]

We approached change detection analysis in two ways: we have compared the images of each of the two analyzed seasons from 1984 to 2015, but we have also looked at changes between one season and another, within a year. The changes of each class surface for each date are illustrated in Fig. 11, the variations between 1984 and 2015 are presented in Fig. 12, and the DTC maps for each year, in Figs. 7–10. For the easiness of the interpretation discussion, we will refer to the May to June images as belonging to the "wet season" and to the August to September images as "dry season."

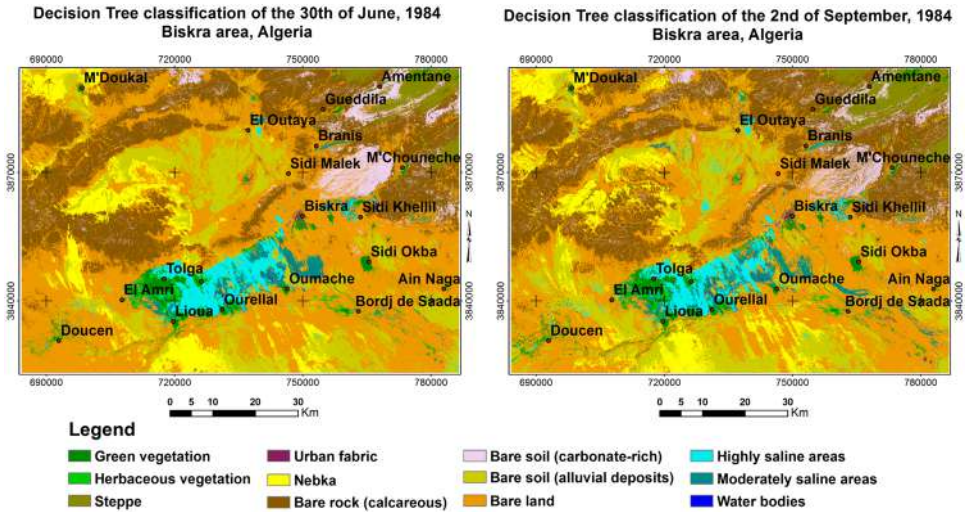

Fig. 7 DTC applied to 1984 images.

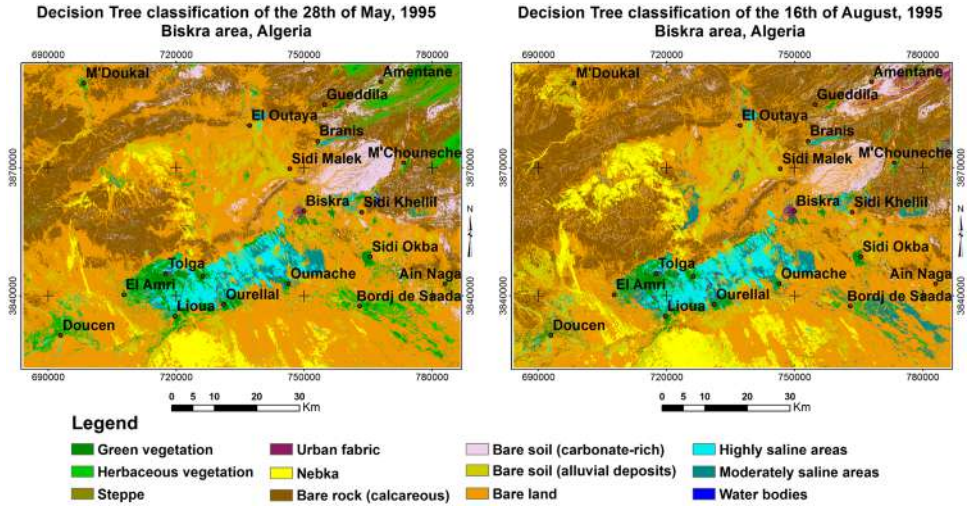

Fig. 8 DTC applied to 1995 images.

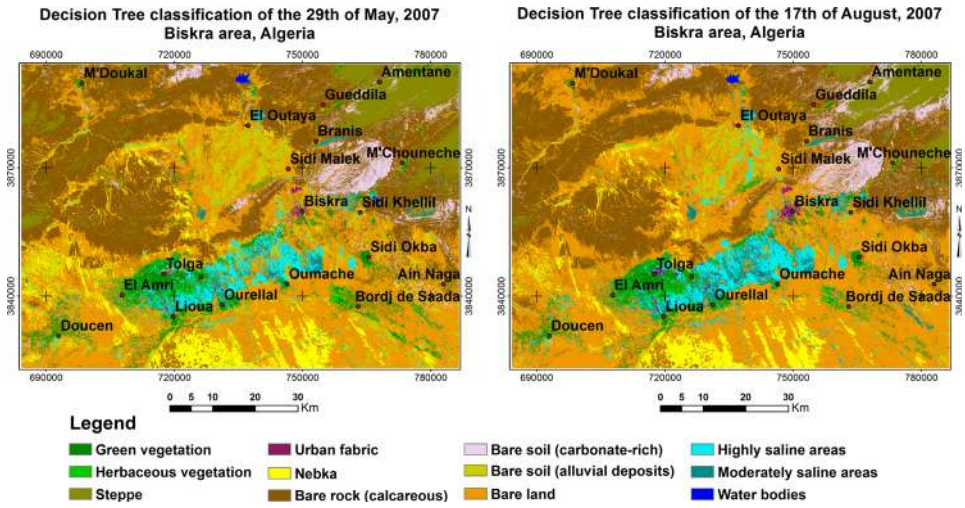

Fig. 9 DTC applied to 2007 images.

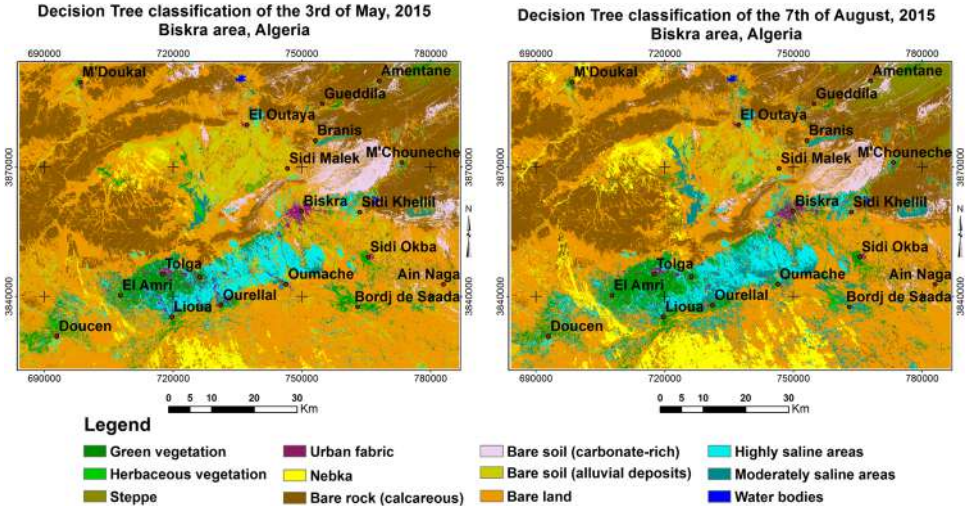

Fig. 10 DTC applied to 2015 images.

From the intraannual point of view, in all years, changes that occur between the end of the wet season and the end of the dry season maintain a similar pattern of change. More specifically, classes that are interchangeable remain as follows: highly saline areas have the most frequent interchange with moderately saline areas, alluvial deposits, and herbaceous vegetation classes (decreasing in 1995, by 1.53% and in 2015 by 1.69% and increasing in 2007 by 17.63%); moderately saline areas mostly interchange with highly saline areas, urban fabric, bare land, and herbaceous vegetation (with an increase of 60% in 1984, 100% in 1995, 93% in 2007, and 106% in 2015).

As an example of intraannual change, the results of the detection analysis of 30 June and 2 September images of the year 1984 show that the "highly saline areas" class has decreased by 26%, mainly in favor of urban fabric class by 18.7%, alluvial deposits by 4.2%, and herbaceous vegetation by 2.1%, gaining only 1.4% and 1.9% of water bodies and herbaceous vegetation classes, respectively. The total changes, with gains and losses, represent −19.8%.

It must be mentioned that throughout the classification process, both in DTC and in Knepper PCA, there has been a strong spectral confusion between the classes of "highly saline areas" and "water bodies" one (consisting of only one dam lake in the whole image in 1984 and 1995, after which another one is visible after 2007, in the northern part of the area, which is reported to be

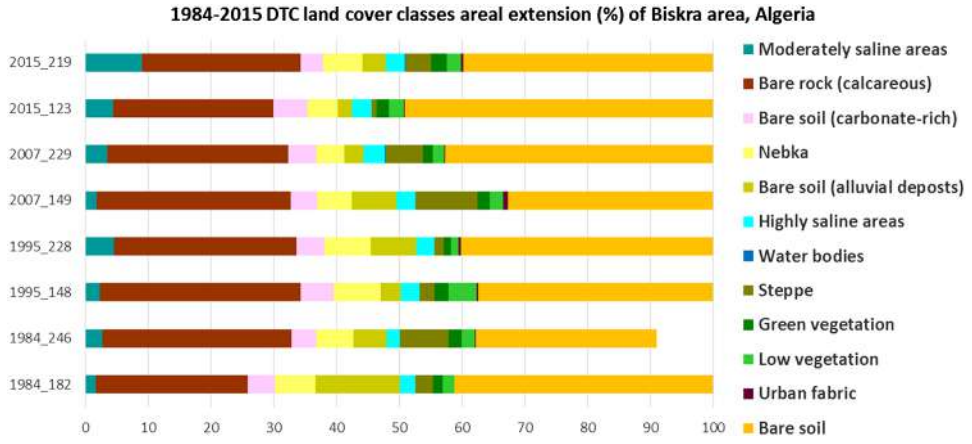

Fig. 11 Class coverage statistics for each analyzed date (percentage).

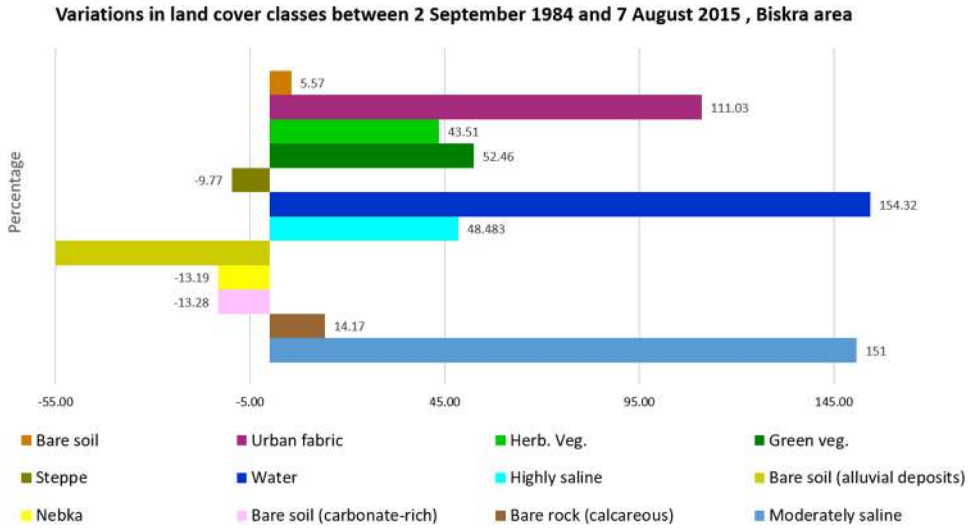

Fig. 12 Variations in land cover classes between September 2, 1984, and August 7, 2015, Biskra area.

due to the construction of a dam). This confusion problem has been solved only throughout the DTC, using the ratio red/infrared, presented as Water Ratio index (WR) in Table 2. The urban fabric presented many difficulties of classification and small insignificant-sized patches are classified under moderately saline areas as it has been noted to have similar spectral behavior to these latter ones in all the analyzed images. However, it maintains this behavior in all analyzed images, and consequently, it does not compromise the classification validity. This spectral confusion has been verified and explained through field observations. Moreover, the experts in the area confirmed that most of the urban structures use construction material extracted from nearby exploitation sites west of Biskra (west-northwest of Lassaad Kara, north of Tolga next to Djebel Gueurn Bou Saïa). As an example of community-based data, this information was also confirmed by geo-tagged photography taken in 2011 and published over Panoramio of Google Earth, entitled "Crushing Plant by UGUR MAKINA."[102] Consequently, we can conclude that, in fact, we are not facing a spectral confusion issue but a correct spectral response of the same type of material.

In the year 1984, the moderately saline areas have an overall increase of 53%, mainly in the disfavor of urban fabric, water bodies, and herbaceous vegetation.

The fact that there is a constant interchange either between "highly saline areas" and "herbaceous vegetation" classes or between "moderately saline areas" and "herbaceous vegetation,"

gives way to the scenario that agricultural practices have the tendency to intensify the salinization processes. This is argued by the fact that more that 80% of the "herbaceous vegetation" class surface correspond to agricultural areas and parcels of cultivated land, in all images. These are mostly recognizable by their rectangular shape, that may or may not present chlorophyll response, and, in some images, by the presence of humidity/water or reworked land hues. Throughout the years, as these cultivated parcels expand, patches of saline soil expand and/or new ones appear in the vicinity of these parcels. These are mainly found in: (1) the Doucen area and around the Tolga Oasis, especially in the El Amri area (Occidental Zab), and (2) the extended agricultural area between Sidi Okba and Ain Naga (Oriental Zab), as can be observed in Fig. 10. The human influence is mainly due to the method of irrigation and the quality of water with high salt concentrations and the manner of field exploitation, which is incompatible with its vocation.[18] Thus, our findings are compatible with those of Mostephaoui et al.[18] who underline that gypsiferous soils are very fragile and easily eroded because of low organic matter content, poor structure, and sparse vegetation cover. Gypsum and gypsiferous deposits cause impervious layers to hinder the growth of plant roots and that soil will be less productive. They emphasize the fact that gypseous soils should have a specific management practice when using gypseous lands for agriculture or urban developments (Ref. 18 and the references within).

Concerning the interannual change analysis, the main trends observed from the change detection statistics are that the "herbaceous vegetation" class presents a major increase (of 34%) in the disfavor of the "green vegetation" class when comparing the 1984 and 2015 images dated at the beginning of the dry season. However, a major increase of the "green vegetation" class compared to "herbaceous vegetation" class is noted at the end of the dry season, of the same pair of years. This comes as a natural change as the herbaceous vegetation class tends to be more sensitive to lack of rainfall and high temperature, as opposed to the green vegetation class which is mainly composed of aridity-resistive palm groves, fruit trees, and shrub vegetation.

Change detection results applied to the 1984 and 2015 pair show that, in both seasons, the main classes with which highly saline areas class has interchanged are the classes of (in ascending order) moderately saline areas, urban fabric, herbaceous vegetation, water, bare soils (alluvial deposits), and green vegetation classes. It must be mentioned that both the highly saline areas and moderately saline areas classes have a similar increase trend when comparing the dry seasons of 1984 to 2015 images (of 48% and 150%, respectively) with the wet seasons of 1984 to 2015 images (of 33% and 164%, respectively). In Table 5 and Fig. 12, the change detection statistics of the dry seasons of 1984 and 2015 are presented as an example.

4.6 *Saline Areas Mapping Issues*

In the Biskra area, the spectral analysis showed that the main factors affecting the reflectance of salt-affected soils are quantity and mineralogy of salts, together with soil moisture, color, impurities content, and surface roughness. The mineralogy of carbonate, sulfates, and chloride salts determines the presence or absence of absorption features in the electromagnetic spectrum, associated with internal vibration modes due to excitation of overtones and combination tones of the fundamental anion groups (e.g., HOH, OH^-, CO_3^{2-}, SO_4^{2-}).[84,92,103] The issues encountered in the current study were those related to spectral confusion between saline areas, alluvial clayey material, carbonate-rich soils, and outcropping limestone. Applying solely salinization indices reported as having high accuracy when mapping salinity in similar areas,[13,14,20,90] results were not satisfactory, since clay and salt-rich soils, urban fabric features, bare land and carbonate-rich surfaces identified together with saline areas and other techniques can cope with these issues.[104] The application of both DTC and IsoDATA of Knepper ratios PCA showed satisfactory results but an overall accuracy of around 76.06%, which may be due to the user dependency of the two datasets (DTC, LCLU map) of the total of three employed (the aforementioned ones and Knepper PCA). However, the results confirm that surface features common in drylands, such as braided stream beds, eroded terrain surfaces with truncated soils, and nonsaline salt-rich structural crusts, can generate high levels of reflectance, similar to those of areas with high salt concentration, as stated by Ref. 84.

Table 5 Example of change detection statistics: 2 September 1984 and 7 August 2015 change analysis.

%	Moderately saline	Bare rock (calcareous)/ mountains	Bare soil (carbonate rich)	Nebka	Bare soil (alluvial deposits)	Highly saline	Water	Steppe	Green veg.	Herb. veg.	Urban fabric	Bare soil
Moderately saline	37.55	0.37	0.16	1.16	8.23	20.55	5.84	0.33	3.32	12.00	19.59	8.63
Bare rock (calcareous)/ mountains	0.16	81.76	43.34	22.06	2.04	0.04	1.46	29.16	0.40	0.56	1.52	6.66
Bare soil (carbonate rich)	0.06	3.24	48.70	0.14	0.39	0.02	0.66	3.65	0.06	0.11	1.06	1.69
Nebka	0.16	0.76	0.00	36.68	18.75	0.30	0.13	0.01	0.11	0.36	0.01	2.18
Bare soil (alluvial deposits)	1.77	0.10	0.12	0.76	13.07	3.90	0.00	0.04	0.20	1.32	4.75	2.63
Highly saline	31.87	0.21	0.04	0.43	4.40	50.62	5.28	0.03	1.11	5.31	10.69	2.63
Water	0.08	0.01	0.01	0.00	0.04	0.00	76.03	0.00	0.01	0.03	0.25	0.05
Steppe	0.62	0.36	1.46	0.30	0.62	0.29	3.92	61.95	10.65	5.92	1.69	1.04
Green veg.	4.63	0.05	0.07	0.60	0.89	7.94	0.93	1.44	53.07	24.63	2.41	1.76
Herb. veg.	5.19	0.07	0.09	0.65	1.36	7.46	2.46	0.81	17.21	20.19	3.70	1.94
Urban fabric	2.19	0.03	0.10	0.03	0.34	4.25	0.60	0.26	3.60	5.87	30.84	0.82
Bare soil	15.73	13.06	5.91	37.20	49.88	4.62	2.39	2.33	10.27	23.71	23.51	69.97
Class Changes	62.45	18.25	51.30	63.32	86.93	49.38	23.97	38.05	46.93	79.81	69.16	30.03
Image difference	**150.85**	**14.17**	**−13.28**	**−13.19**	**−77.46**	**48.48**	**154.32**	**−9.77**	**52.46**	**43.51**	**111.03**	**5.57**

5 Conclusion

The employment of the DTC has proven to be more flexible and adequate for the extraction of highly and moderately saline areas and major land cover types, as it allows multisource information and higher user control. In this study, we employ both visual and automated classification methods. This methodological approach of two mapping methods proposed in this study was conceived because it is meant to be replicable in areas where historical data are scarce, and the access to acquire field data is limited, either because the areas are remote/large or because of sociopolitical restrictions.

First, the visual interpretation of one Landsat scene of June 9, 2011, was undergone and a detailed LCLU map was generated. This phase was supported by a large set of ancillary data, and the output map was validated with multisource GT points (field, pedological report, Google Earth points). In the second phase, the decision tree was built based on a previous spectral analysis and existing indices assessment and nonetheless, the construction of new ones according to the current purpose. Third, the PCA was applied to Knepper ratios composite, as a support for the decision tree verification. The visually interpreted LCLU map was used for the validation of the 2011 DTC map for all land cover classes. However, GT points were also employed for the validation of the 2011 DTC map, but only for the "highly saline" class. A comparison between the 2011 DTC maps and the IsoDATA classified Knepper ratios' PC images was also undergone, taking into consideration only the "highly saline" class.

The results were compared with IsoDATA classification maps applied to Knepper ratios PCA and were proven to have a substantial advantage over this latter method. Out of a total of 11 indices employed in the DTC construction, five new indices were proposed for the current study. The accuracy assessment of the salinity index (SMI) proposed in this paper for the extraction of highly saline areas was verified through comparison with two other mapping methods, being of around 95%. Applying postclassification change detection (ENVI), the statistics for the 1984 to 2014 diachronic analysis, comprising images acquired at the end of the wet season and at the end of the dry season, have shown an overall increase of 53% of the highly saline areas surface, but no substantial change between the seasons. The "moderately saline areas" class was noted to have variations from one year to another, in terms of fluctuant increase–decrease and also within the same year, as it was observed to be slightly more sensitive to seasonal conditions than the "highly saline areas" class. However, it presented an overall increase of over 100% from 1984 to 2015, but still no substantial change from one season to another. In fact, the results showed that even if we are dealing with a predesert area, the seasonal variations had minimum influence on either highly or moderately saline areas correct delineation. The results showed only a slight interchange between the two classes (of small surfaces) but no issues of correctly identifying, delineating, or being masked by vegetation were observed.

One of the important aspects that emerged from the diachronic series analyses is that the expansion of open field and industrial agriculture practices in the last three decades has led and continues to contribute to a secondary salinization of soils. In the Occidental Zab, the increase in salinized soils correspond to the expansion of phoeniciculture and market gardening (often greenhouse). In the Oriental Zab, the large scale industrial agriculture, which required also a large number of deep wells (given the 200 to 300 m depth of the exploitable groundwater), has caused sporadic local appearance of small patches of salinized surfaces all along the lower slope of the alluvial fan area.

Appendix: Land Cover and Land Use Map Nomenclature (Fourth Level of Detail, Upper Levels Correspond to CORINE Land Cover Nomenclature)

1.1.1.1. Areas of urban centers;
1.1.1.2. Areas of ancient cores;
1.1.2.1. Discontinuous built-up areas with areas of bare soil;
1.1.2.2. Discontinuous built-up areas with areas of Palm groves or Oasis vegetation;
1.1.3.1. Peripheral urban wasteland;
1.2.1.1. Industrial or commercial units;
1.2.4.1. Airports with artificial surfaces of runways;
1.3.1.1. Quarries and open-cast mines;

1.3.3.1. Construction sites;
1.4.2.1. Sport facilities;
2.1.2.1. Permanently irrigated land;
2.2.2.1. Primary Oasis;
2.2.2.2. Secondary Oasis;
2.4.1.1. Annual crops associated with Palm groves;
2.4.1.2. Annual crops associated with other permanent crops;
2.4.1.3. Arable land associated with greenhouses (maraicheres) with significant areas of Palm groves;
2.4.1.4. Discontinuous arable land associated with Palm plantations;
2.4.2.1. Complex cultivation patterns;
2.4.3.1. Agricultural areas with significant share of natural vegetation, and with prevalence of annual crops in late stages of phenophase;
2.4.3.2. Agricultural areas with visible cultivation pattern, with significant share of natural vegetation, with the prevalence of annual crops in early phenological stage or not yet sprouted (ploughted land prevailingly);
3.2.1.1. Natural, open grassland prevailingly without shrubs (<20%);
3.2.1.2. Open grassland with shrubs;
3.2.1.3. Riparian vegetation;
3.2.3.1. Mixed xerophilous vegetation;
3.2.3.2. Halophile vegetation;
3.3.1.3. River banks/beds sandy, dry Wadis;
3.3.2.1. Hamada;
3.3.2.2. Bare rock/soil, usually saline/alkali;
3.3.3.1. Nebkas (phytogenic coppice dunes);
3.3.3.2. Sparse vegetation on rocks/hamada;
3.3.3.3. Sparse vegetation on saline/alkali soils;
3.3.3.4. Sparse vegetated alluvial fans;
4.1.1.4. Saline (alkali) inland marshes without reed beds (<20%) and with other water plants;
4.1.1.5. Sebkha/daia;
4.1.1.6. Temporary humid areas floodable areas with no or little vegetation;
5.1.1.1. Wadi;
5.1.2.1. Water bodies.

Acknowledgments

This study was developed within the frame of the doctoral research (2013-2016) of Gabriela Mihaela Afrasinei, financed by the Italian Ministry of Education, Universities and Research (MIUR), in "Soil preservation, environmental vulnerability, and hydrogeological protection" of the PhD school in Environmental and Land Sciences and Engineering, University of Cagliari (Italy). We wish to express our sincere appreciation to the WADIS-MAR project for the possibility of conducting the current research and the TeleGIS Laboratory group of the University of Cagliari (Italy) for their invaluable support. We also wish to thank the Algerian WADIS-MAR partners, "Institut Technique de Développement de l'Agronomie Saharienne," Biskra, Algeria (ITDAS), and "Agence Nationale des Ressources Hydrauliques," Algeria (ANRH) for the provided data and collaboration. Acknowledgments are also due to the Spatial Analysis Laboratory of the University of Wollongong, Australia, for their support provided during the undertaken research program. We also wish to acknowledge the invaluable support and contribution of PhD Geologist Marco Pistis of the University of Cagliari, for the sedimentological, mineralogical and geological interpretation and insights.

References

1. A. A. A. Aldabaa et al., "Combination of proximal and remote sensing methods for rapid soil salinity quantification," *Geoderma* **239–240**, 34–46 (2015).
2. M. T. Hoffman et al., *Land Degradation and Desertification*, Report, Intergovernmental Panel on Climate Change (IPCC), Intergovernmental Panel on Climate Change (IPCC) (1995).

3. P. D'Odorico et al., "Global desertification: drivers and feedbacks," *Adv. Water Resour.* **51**, 326–344 (2013).
4. FAO, "Soil salinity assessment," Report, FAO (1999).
5. FAO, "Advances in the assessment and monitoring of salinization and status of biosaline agriculture. Reports of expert consultation held in Dubai, United Emirates, 26–29 November 2007," Report, Rome (2009).
6. N. Varghese and N. P. Singh, "Linkages between land use changes, desertification and human development in the Thar Desert Region of India," *Land Use Policy* **51**, 18–25 (2016).
7. C. Kosmas et al., "Evaluation and selection of indicators for land degradation and desertification monitoring: methodological approach," *Environ. Manage.* **54**(5), 951–970 (2013).
8. E. Asfaw, K. V. Suryabhagavan, and M. Argaw, "Soil salinity modeling and mapping using remote sensing and GIS: the case of Wonji sugar cane irrigation farm, Ethiopia," *J. Saudi Soc. Agric. Sci.* (2016).
9. M. Lamchin et al., "Assessment of land cover change and desertification using remote sensing technology in a local region of Mongolia," *Adv. Space Res.* **57**(1), 64–77 (2016).
10. R. Escadafal et al., "First appraisal of the current structure of research on land and soil degradation as evidenced by bibliometric analysis of publications on desertification," *Land Degrad. Dev.* **26**(5), 413–422 (2015).
11. M. H. Fares and C. G. Philip, "Characterization of salt-crust build-up and soil salinization in the United Arab emirates by means of field and remote sensing techniques," in *Remote Sensing of Soil Salinization*, G. Metternicht and A. Zinck, Ed., pp. 141–152, Taylor & Francis Group, USA (2008).
12. A. A. Elnaggar and J. S. Noller, "Application of remote-sensing data and decision-tree analysis to mapping salt-affected soils over large areas," *Remote Sens.* **2**(1), 151–165 (2010).
13. A. A. Masoud, "Predicting salt abundance in slightly saline soils from Landsat ETM+ imagery using spectral mixture analysis and soil spectrometry," *Geoderma* **217–218**, 45–56 (2014).
14. A. A. Masoud and K. Koike, "Arid land salinization detected by remotely-sensed land-cover changes: a case study in the Siwa region, NW Egypt," *J. Arid Environ.* **66**(1), 151–167 (2006).
15. C. Bowyer et al., "Economic and scientific policy land degradation and desertification," in *Economic and Scientific Policy of the European Parliament* (2009).
16. I. Yahiaoui et al., "Soil salinity prediction in the Lower Cheliff plain (Algeria) based on remote sensing and topographic feature analysis," *J. Arid Land* **7**(6), 794–805 (2015).
17. I. Yahiaoui et al., "Digital mapping of landscapes based on soil morphology in the plain of Lower-Cheliff (Algeria): application of remote-sensing," (2016).
18. T. Mostephaoui, R. Bensaid, and M. L. Saker, "Localization and delimitation of the arid soils by remote sensing and in-situ measurements in an arid area: case of Oued Djedi watershed, Biskra, Algeria," *World Appl. Sci. J.* **24**(3), 370–382 (2013).
19. A. Abbas et al., "Characterizing soil salinity in irrigated agriculture using a remote sensing approach," *Phys. Chem. Earth* **55–57**, 43–52 (2013).
20. A. Allbed and L. Kumar, "Soil salinity mapping and monitoring in arid and semi-arid regions using remote sensing technology: a review," *Adv. Remote Sens.* **2**(4), 373–385 (2013).
21. A. Allbed, L. Kumar, and Y. Y. Aldakheel, "Assessing soil salinity using soil salinity and vegetation indices derived from IKONOS high-spatial resolution imageries: applications in a date palm dominated region," *Geoderma* **230–231**, 1–8 (2014).
22. S. Dhruba Pikha, "Mapping salinity hazard," in *Remote Sensing of Soil Salinization*, G. Metternicht and A. Zinck, Ed., pp. 257–270, Taylor & Francis Group, USA (2008).
23. Z. Zhang et al., "A 2010 update of National Land Use/Cover Database of China at 1:100000 scale using medium spatial resolution satellite images," *Remote Sens. Environ.* **149**, 142–154 (2014).

24. T. Ceccarelli, "Land cover data from Landsat single-date imagery: an approach integrating pixel-based and object-based classifiers," *Eur. J. Remote Sens.* **46**, 699–717 (2013).
25. M. Li, "A review of remote sensing image classification techniques: the role of spatio-contextual information," *Eur. J. Remote Sens.* **47**, 389–411 (2014).
26. S. Avelar and P. Tokarczyk, "Analysis of land use and land cover change in a coastal area of Rio de Janeiro using high-resolution remotely sensed data," *J. Appl. Remote Sens.* **8**(1), 083631 (2014).
27. Z. Zhang et al., "A 2010 update of National Land Use/Cover Database of China at 1:100000 scale using medium spatial resolution satellite images," *Remote Sens. Environ.* **149**, 142–154 (2014).
28. S. Aleksandrowicz et al., "Change detection algorithm for the production of land cover change maps over the European Union countries," *Remote Sens.* **6**(7), 5976–5994 (2014).
29. P. Olofsson et al., "Good practices for estimating area and assessing accuracy of land change," *Remote Sens. Environ.* **148**, 42–57 (2014).
30. Z. Zhu and C. E. Woodcock, "Continuous change detection and classification of land cover using all available Landsat data," *Remote Sens. Environ.* **144**, 152–171 (2014).
31. J. Farifteh et al., "Spectral characteristics of salt-affected soils: a laboratory experiment," *Geoderma* **145**(3–4), 196–206 (2008).
32. N. M. Khan et al., "Assessment of hydrosaline land degradation by using a simple approach of remote sensing indicators," *Agric. Water Manage.* **77**(1–3), 96–109 (2005).
33. P. Rao, S. Chen, and K. Sun, "Improved classification of soil salinity by decision tree on remotely sensed images," *Proc. SPIE* **6027**, 60273K (2006).
34. C. H. Matthew, "Classification trees and mixed pixel training data," in *Remote Sensing of Land Use and Land Cover*, C. P. Giri, Ed., pp. 127–137, Taylor & Francis Group, USA (2012).
35. P. K. Srimani and N. Prasad, "Decision tree classification model for land use and land cover mapping—a case study," *Int. J. Curr. Res.* **4**(5), 177–181 (2012).
36. M. Pal and P. M. Mather, "An assessment of the effectiveness of decision tree methods for land cover classification," *Remote Sens. Environ.* **86**(4), 554–565 (2003).
37. M. Pal, "Advanced algorithms for land use and cover classification," in *Advances in Mapping from Remote Sensor Imagery*, X. Yang and J. Li, Ed., pp. 70–82, Taylor & Francis Group, USA (2012).
38. M. J. Cracknell and A. M. Reading, "Geological mapping using remote sensing data: a comparison of five machine learning algorithms, their response to variations in the spatial distribution of training data and the use of explicit spatial information," *Comput. Geosci.* **63**, 22–33 (2014).
39. R. Sharma, A. Ghosh, and P. K. Joshi, "Decision tree approach for classification of remotely sensed satellite data using open source support," *J. Earth Syst. Sci.* **122**(5), 1237–1247 (2013).
40. J. R. Otukei and T. Blaschke, "Land cover change assessment using decision trees, support vector machines and maximum likelihood classification algorithms," *Int. J. Appl. Earth Obs. Geoinf.* **12**(Suppl. 0), S27–S31 (2010).
41. J. Rogan, J. Franklin, and D. A. Roberts, "A comparison of methods for monitoring multitemporal vegetation change using Thematic Mapper imagery," *Remote Sens. Environ.* **80**(1), 143–156 (2002).
42. J. Rogan et al., "Mapping land-cover modifications over large areas: a comparison of machine learning algorithms," *Remote Sens. Environ.* **112**(5), 2272–2283 (2008).
43. G.-M. Afrasinei et al., "Classification methods for detecting and evaluating changes in desertification-related features in arid and semiarid environments," *Eur. Mediterr. J. Environ. Integr.*, Springer (2016) in press.
44. R. L. Langford, "Temporal merging of remote sensing data to enhance spectral regolith, lithological and alteration patterns for regional mineral exploration," *Ore Geol. Rev.* **68**, 14–29 (2015).
45. A. Dehni and M. Lounis, "Remote sensing techniques for salt affected soil mapping: application to the Oran region of Algeria," *Proc. Eng.* **33**, 188–198 (2012).

46. Y.-L. Weng, P. Gong, and Z.-L. Zhu, "A spectral index for estimating soil salinity in the yellow river delta region of china using eO-1 hyperion data," *Pedosphere* **20**(3), 378–388 (2010).
47. F. Jamshid, "Model-based integrated methods for quantitative estimation of soil salinity from hyperspectral remote sensing data," in *Remote Sensing of Soil Salinization*, CRC Press (2008).
48. J. Farifteh, A. Farshad, and R. J. George, "Assessing salt-affected soils using remote sensing, solute modelling, and geophysics," *Geoderma* **130**(3–4), 191–206 (2006).
49. R. L. Dehaan and G. R. Taylor, "Field-derived spectra of salinized soils and vegetation as indicators of irrigation-induced soil salinization," *Remote Sens. Environ.* **80**, 406–417 (2002).
50. K. Amri, Y. Mahdjoub, and L. Guergour, "Use of Landsat 7 ETM+ for lithological and structural mapping of Wadi Afara Heouine area (Tahifet–Central Hoggar, Algeria)," *Arabian J. Geosci.* **4**(7–8), 1273–1287 (2010).
51. F. D. van der Meer et al., "Multi- and hyperspectral geologic remote sensing: a review," *Int. J. Appl. Earth Obs. Geoinf.* **14**(1), 112–128 (2012).
52. Q. Kang et al., "Remote sensing application of soil salinization based on multi-source images," *Proc. SPIE* **6045**, 60452V (2005).
53. G.-M. Afrasinei et al., "Metodologia per la caratterizzazione spettrale delle superfici saline e delle aree interessate da aspersioni sabbiose tramite proximal sensing e remote sensing in Tunisia," *ASITA* 11–18 (2015).
54. D. E. Mitchell, "Identifying salinization through multispectral band analysis: Lake Urmia, Iran," Thesis, Ryerson University, Canada (2014).
55. H. Fu et al., "Land salinization classification method using Landsat TM in western Jilin Province of China," *Proc. SPIE* **9220**, 92200U (2014).
56. M. Bouaziz, J. Matschullat, and R. Gloaguen, "Improved remote sensing detection of soil salinity from a semi-arid climate in Northeast Brazil," *C. R. Geosci.* **343**(11–12), 795–803 (2011).
57. F. Nutini et al., "Land-use and land-cover change detection in a semi-arid area of Niger using multi-temporal analysis of Landsat images," *Int. J. Remote Sens.* **34**(13), 4769–4790 (2013).
58. J. A. Zinck and G. Metternicht, "Soil salinity and salinization hazard," in *Remote Sensing of Soil Salinization*, G. Metternicht and J. A. Zinck, Ed., pp. 3–18, Taylor & Francis Group, USA (2008).
59. G. I. Metternicht and J. A. Zinck, "Remote sensing of soil salinity: potentials and constraints," *Remote Sens. Environ.* **85**(1), 1–20 (2003).
60. Nucleo Ricerca Desertificazione, University of Sassari, "WADIS-MAR Demonstration Project," 2017, www.wadismar.eu (2014).
61. G. Ghiglieri et al., "Design of artificial aquifer recharge systems in dry regions of Maghreb (North Africa)," in *FlowPath2014—National Meeting on Hydrogeology FlowPath20*, Dipartimento di Scienze Ecologiche e Biologiche and U. Degli and S. della Tuscia, Eds., Dipartimento di Scienze Ecologiche e Biologiche, Università degli Studi della Tuscia, Viterbo (2014).
62. C. Arras et al., "Evaluation and validation of SRTMGL1 and ASTER GDEM2 for two Maghreb regions (Biskra, Algeria and Medenine, Tunisia)," in *ILDAC2015 Book Proc. Integrated*, Springer (2016).
63. A. Bougherara and B. Lacaze, "Etude preliminaire des images Landsat et Alsat pour le suivi des mutations agraires des Ziban (extrême nord-est du Sahara algérien) de 1973 à 2007," in Journées d'Animation Scientifique (JAS09) de l'AUF Alger, Journées d'Animation Scientifique (JAS09) de l'AUF Alger, Journées d'Animation Scientifique (JAS09) de l'AUF Alger (2009).
64. C. Buttau et al., "Studio geologico strutturale per indagini idrogeologiche dell'area compresa tra le regioni di Batna e Biskra (NE Algeria)," *Rend Online Soc Geol. It* **29**, 13–16 (2013).
65. M. de l'Hydraulique Algerienne, "Notice explicative de la Carte Hydrogeologique de Biskra au 1/200.000," Map, Ministere de l'Hydraulique Algerienne MdH, Alger, Algeria (1980).

66. C. Arras et al., "Preliminary results of a 3-D groundwater flow model in an arid region of NE Algeria using PMWin: the Inféro-flux phreatic aquifer (Biskra)," *Rend. Online Soc. Geol. It.*, **41**, 18–21 (2016).
67. Tutiempo Network, S.L., "Climate Biskra. Climate data: 1943 -2016," 2017, www.tutiempo.org (2014).
68. M. Hamid Reza and R. Majid Shadman, "Decision Tree Land Use/Land Cover Change Detection of Khoram Abad City Using Landsat Imagery and Ancillary SRTM Data," in *Scholars Research Library (Annals of Biological Research)*, pp. 4045–4053 (2012).
69. G. Yao et al., "Implementation of the CORINE land use classification in the regional climate model REMO," *Boreal Environ. Res.* **20**(2), 261–282 (2015).
70. G. Jaffrain, "CORINE land cover outside of Europe. Nomenclature adaptation to other biogeographical regions," Report, Universidad de Malaga, ETCSIA, Spain (2011).
71. J. Feranec et al., "The 4th level corine land cover nomenclature for the phare countries," Report, Institute of Geography, Slovak Academy of Sciences, Bratislava, Slovak Republic (2000).
72. G. Büttner et al., "National CORINE Land Cover mapping at scale 1:50.000 in Hungary," Report, FÖMI Remote Sensing Centre, Budapest, Hungary (2000).
73. ETC/LC and E. E. Agency, "CORINE Land cover. Technical guide," Report, ETC/LC, European Environment Agency (1999).
74. X. Pons et al., "Automatic and improved radiometric correction of Landsat imagery using reference values from MODIS surface reflectance images," *Int. J. Appl. Earth Obs. Geoinf.* **33**, 243–254 (2014).
75. S. Vanonckelen, S. Lhermitte, and A. Van Rompaey, "The effect of atmospheric and topographic correction methods on land cover classification accuracy," *Int. J. Appl. Earth Obs. Geoinf.* **24**, 9–21 (2013).
76. S. Vanonckelen et al., "Performance of atmospheric and topographic correction methods on Landsat imagery in mountain areas," *Int. J. Remote Sens.* **35**(13), 4952–4972 (2014).
77. IDRISI, *Introduction to Remote Sensing and Image Processing*, Pamphlet.
78. V. L. Mulder et al., "The use of remote sensing in soil and terrain mapping—a review," *Geoderma* **162**(1–2), 1–19 (2011).
79. D. Lu and Q. Weng, "Review article: a survey of image classification methods and techniques for improving classification performance," *Int. J. Remote Sens.* **28**(5), 823–870 (2007).
80. J. Rogan et al., "Remote sensing for mapping and monitoring land-cover and land-use change," *Progr. Plann.* **61**(4), 267 (2004).
81. P. Darren et al., "Supervised classification approaches for the development of land-cover time series," in *Remote Sensing of Land Use and Land Cover*, pp. 177–190, Taylor & Francis Group, USA (2012).
82. M. T. Melis et al., "Caratterizzazione spettrale delle aree interessate da salinizzazione nel bacino del Oued Biskra in Algeria a supporto delle politiche di gestione dell'acqua nell'ambito del progetto WADIS-MAR," in *Atti 17a Conf. Nazionale ASITA*, 5–7 November 2013, pp. 977–982, ASITA, Riva del Garda (2013).
83. V. L. Mulder et al., "Characterizing regional soil mineral composition using spectroscopy and geostatistics," *Remote Sens. Environ.* **139**, 415–429 (2013).
84. G. Metternicht and J. A. Zinck, "Spectral behavior of salt types," in *Remote Sensing of Soil Salinization*, CRC Press (2008).
85. A. Schneider, "Monitoring land cover change in urban and peri-urban areas using dense time stacks of Landsat satellite data and a data mining approach," *Remote Sens. Environ.* **124**, 689–704 (2012).
86. A. E. K. Douaoui, H. Nicolas, and C. Walter, "Detecting salinity hazards within a semiarid context by means of combining soil and remote-sensing data," *Geoderma* **134**(1–2), 217–230 (2006).
87. R. Yu et al., "Analysis of salinization dynamics by remote sensing in Hetao Irrigation District of North China," *Agric. Water Manage.* **97**(12), 1952–1960 (2010).

88. G. M. Afrasinei et al., "Diachronic analysis of salt-affected areas using remote sensing techniques: the case study of Biskra area, Algeria," *Proc. SPIE* **9644**, 96441D (2015).
89. B. Mia and Y. Fujimitsu, "Mapping hydrothermal altered mineral deposits using Landsat 7 ETM+ image in and around Kuju volcano, Kyushu, Japan," *J. Earth Syst. Sci.* **121**(4), 1049–1057 (2012).
90. N. M. Khan et al., "Mapping salt-affected soils using remote sensing indicators—a simple approach with the use of GIS IDRISI -," in *22nd Asian Conf. on Remote Sensing* (2001).
91. A. Sidike, S. Zhao, and Y. Wen, "Estimating soil salinity in Pingluo County of China using QuickBird data and soil reflectance spectra," *Int. J. Appl. Earth Obs. Geoinf.* **26**, 156–175 (2014).
92. R. N. Clark, "Spectroscopy of rocks and minerals, and principles of spectroscopy," in *Manual on Remote Sensing, Remote Sensing for the Earth Sciences*, Vol. **3**, A. N. Rencz, Ed., pp. 3–58, John Wiley and Sons, New York (1999).
93. D. H. Knepper, "Mapping hydrothermal alteration with landsat thematic mapper data," in *Remote Sensing in Exploration Geology: Golden*, K. Lee et al., Ed., American Geophysical Union, Washington, D.C. (1989).
94. M. Marconcini, D. Fernandez-Prieto, and T. Buchholz, "Targeted land-cover classification," *IEEE Trans. Geosci. Remote Sens.* **52**(7), 4173–4193 (2014).
95. F. Nutini et al., "Land-use and land-cover change detection in a semi-arid area of Niger using multi-temporal analysis of Landsat images," *Int. J. Remote Sens.* **34**(13), 4769–4790 (2013).
96. R. A. Raja Alagu et al., "Wavelet based post classification change detection technique for urban growth monitoring," *J. Indian Soc. Remote Sens.* **41**(1), 35–43 (2013).
97. M. M. El-Hattab, "Applying post classification change detection technique to monitor an Egyptian coastal zone (Abu Qir Bay)," *Egypt. J. Remote Sens. Space Sci.* **19**(1), 23–36 (2016).
98. D. Woo and V. D. Do, "Post-classification change detection of high resolution satellite images using Adaboost classifier multi-class Adaboost Algorithm," *Adv. Sci. Technol. Lett.* **117**, 34–38 (2015).
99. R. Latifovic and D. Pouliot, "Approaches to IPCC land-use and land-use change reporting in agriculture areas with remote sensing," *J. Chem. Inf. Model.* **53**(9), 1689–1699 (2013).
100. P. Serra, X. Pons, and D. Saurí, "Post-classification change detection with data from different sensors: some accuracy considerations," *Int. J. Remote Sens.* **24**(23), 4975–4976 (2003).
101. A. Singh, "Digital change detection techniques using remotely-sensed data," *Int. J. Remote Sens.* **10**(6), 989–1003 (1989).
102. Uğur Makina, "Crushing-screening-washing-stockpilling plants," 2017, http://www.ugurmak.com.tr/ (2014).
103. I. Szabolcs, *Salt Affected Soils*, p. 274, CRC Press, Boca Raton, Florida (1989).
104. A. Bendib, H. Dridi, and M. I. Kalla, "Contribution of Landsat 8 data for the estimation of land surface temperature in Batna city, Eastern Algeria," *JOUR, Geocarto Int.*, pp. 1–11, Taylor & Francis (2016).

Gabriela M. Afrasinei: Biography is not available.

Maria T. Melis is an adjunct professor in GIS and the technical responsible for the "TeleGIS" Remote Sensing Laboratory, University of Cagliari, Italy. Her research focuses on remote sensing applied to geological/land cover/geomorphological analysis, publishing +50 papers. She is the vice president of the Italian Association of Remote Sensing (since 2006) and member of the Scientific Council of ASITA. Since 2006, she has been working for the European Commission FP6, FP7, and Horizon2020 as an expert evaluator.

Cristina Buttau received her master's and PhD degrees in geology from the University of Cagliari, Italy. She has more than 10 years of experience in structural geology, 3D geological

and geological data processing for hydrological applications. She has authored and coauthored 4 articles in peer-reviewed scientific journals, 2 geological maps and +30 conference papers. Her current research focuses on the interpretation of existing and new geological and hydrogeological data for 3D hydrogeological modeling.

John M. Bradd is the director and principal hydrogeologist of Hydrogeological Solutions Pty. Ltd. and a principal honorary fellow at the University of Wollongong, Australia. He was a reviewer for two Elsevier journals and the *Australian Journal of Earth Sciences*. He is affiliated with the International Association of Hydrogeologists. He has extensive experience in groundwater, environmental, and water resource investigations in Australia and Southeast Asia. He authored/coauthored +20 scientific articles and +13 technical reports.

Claudio Arras received his master's degree in geology from the University of Cagliari, Italy, in 2013. His current PhD research focuses on the reconstruction of 3D hydrogeological models finalized at the development of a groundwater flow numerical model for the management of groundwater resources in arid and semiarid regions. He authored and coauthored 3 articles in peer-reviewed scientific journals and more than ten conference papers.

Giorgio Ghiglieri is an associate professor of hydrogeology and engineering geology at the University of Cagliari, Italy. His expertise includes hydrogeology, protection of aquifers from contamination, managed aquifer recharge systems, landslide hazard, and desertification. He has more than 25 years of experience in several national and international research project collaboration and coordination in Italy and Africa (Ethiopia, Tanzania, Mauritania, Benin, Tunisia and Algeria). He authored and coauthored more than 30 scientific articles and +20 conference papers.